ORIGINAL ARTICLE

Green synthesis of AgCoFe$_2$O$_4$@Ch/AC as a recyclable, magnetic nanohybrid heterogeneous catalyst in photodegradation of ceftriaxone from aqueous solutions with effluent bioassay

Mohammad Hossein Amiri Fard[1,2] · Alireza Nasiri[1] · Hasti Daraei[1,2]

Abstract

Ceftriaxone (CFTR) is among the most commonly used antibiotics in the treatment of different types of bacterial infections and widespread pneumonias. It was also known as one of the most frequently prescribed antibiotics during the Corona pandemic. This drug has a longer half-life than other antibiotics. In this research, the heterogeneous magnetic nanophotocatalyst AgCoFe$_2$O$_4$@Chitosan(Ch)/activated carbon (AC) was synthesized by co-precipitation method under microwave waves. The catalyst structure was characterized by XRD, FTIR, FESEM, EDS, mapping, line scan, BET, VSM and DRS analyzers. Then, the effect of pH, CFTR concentration, nanophotocatalyst dose and irradiation time on the photocatalytic process efficiency was investigated. The analyses showed that the catalyst was synthesized on a nanometer scale, high surface area (60.044 m^2/g), high magnetic strength (Ms = 10.39 emu/g) and appropriate optical activity with band gap (3.1 eV). The highest removal efficiency at pH = 3, CFTR concentration of 5 mg/L, dose of 0.24 g/L, and irradiation time of 60 min was obtained at 98.8% and 79.01% for synthetic and real wastewater samples, respectively. The reaction kinetics followed the *pseudo*-first-order and Langmuir–Hinshelwood kinetic models with K_C = 0.23 mg/L min and K_{L-H} = 0.168 L/mg. The recovered catalyst was able to remove CFTR with an efficiency of 80.16% after 4 reuse cycles. The results of scavenger radical tests showed that the main active radical species was ·OH. The obtained results from the effluent toxicity on the germination index of lettuce, watercress, radish and tomato seeds showed a significant reduction in the environmental hazards of the effluent. Due to the high efficiency, this nanophotocatalyst can be used for the treatment of pharmaceutical and hospital wastewaters, and the effluent has the least toxicity for the environment.

Keywords Magnetic nanophotocatalyst · Ceftriaxone · Water treatment · Photodegradation

Introduction

Today, the discharge of wastewater containing pharmaceutical residues, especially antibiotics, into the environment and their destructive effects on aquatic ecosystems and microorganisms has been raised as a global concern (Kestioğlu et al. 2005). Since antibiotics have a long half-life, they have been found abundantly in the effluents of wastewater treatment plants and water sources (Yazdanbakhsh et al. 2016a). The presence of antibiotics in the environment can inhibit the activity of beneficial bacteria and also indirectly cause resistance, genetic and phenotypic changes in microbial communities (Daraei et al. 2021). Antibiotics enter aquatic environments from various routes such as direct discharge from pharmaceutical industries, hospitals and medical centers, sewage treatment plants, human and animal excreta, etc. (Yazdanbakhsh et al. 2016b). Ceftriaxone (C$_{18}$H$_{16}$N$_8$Na$_2$O$_7$S$_3$) is one of the common cephalosporin antibiotics with a long half-life. Ceftriaxone (CFTR) is usually used to treat respiratory infections, skin infections, pneumonia, etc., and it was one of the most widely used antibiotics during the Corona epidemic in 2019 (Chang Pitter et al. 2022). Studies have shown that 33–67% of ceftriaxone is excreted unchanged through the kidneys (Nishioka et al. 2022).

✉ Hasti Daraei
hasti.daraei@yahoo.com; h.daraei@kmu.ac.ir

[1] Environmental Health Engineering Research Center, Kerman University of Medical Sciences, Kerman, Iran

[2] Department of Environmental Health Engineering, Faculty of Public Health, Kerman University of Medical Sciences, Kerman, Iran

CFTR has very low biodegradability and their entry into the biological processes of WWTPs can lead to a decrease in their performance due to damage to cyanobacteria, algae and microorganisms. Common wastewater treatment processes are classified into three categories, namely physical (filtration, absorption, extraction, etc.), biological (aerobic, anaerobic activated sludge) and chemical (oxidation, ion exchange, chemical precipitation, etc.), which are not able to completely remove antibiotics. These processes also have disadvantages such as high energy consumption, high cost, membrane clogging, equipment corrosion, complex biological process control, incomplete decomposition and production of toxic intermediates (Yazdanbakhsh et al. 2016b). On the other hand, advanced oxidation processes (AOPs) have been considered due to their high efficiency in the destruction of complex pollutants, no sludge production, no toxicity, high oxidation power, low cost and simple application (Daraei et al. 2023). In AOPs, highly oxidizing radicals such as $^{\cdot}OH$, SO_4^{-} and O_2^{-} are produced and lead to the destruction and transformation of pollutants into simpler and less dangerous molecules such as water, carbon dioxide and mineral ions (Firoozi et al. 2023).

The photocatalytic process is one of the most widely used advanced oxidation methods in which metal oxides or their composites are used to increase the efficiency of the process and produce more active free radicals (Daraei et al. 2023). So far, various non-magnetic nanocatalysts (such as TiO_2, MnO_2, ZnO and SiO_2) have been used to remove impurities from aqueous solutions that their most important disadvantage is their difficult separation from the solution and the interruption of the process. To solve this problem, nanocatalysts with magnetic properties can be synthesized and used (Joshi et al. 2022). Other advantages of magnetic nanocatalysts include facile synthesis and separation, non-toxicity, high stability and recyclability (Majlesi and Daraei 2016).

Recently, magnetic nanocatalysts such as $ZnFe_2O_4$@Carboxymethyl cellulose (CMC), $CuFe_2O_4$@Methylcellulose (MC) and $CoFe_2O_4$@AC/H_2O_2 have been used to remove pharmaceutical contaminants from aqueous solutions (Nasiri et al. 2019; Rajabi et al. 2022; Malakootian et al. 2020). The presence of various transition metals with different oxidation and reduction potentials in the structure of these catalysts causes changes in their catalytic performance during the advanced oxidation process. Most of the Ag-based catalysts could exhibit strong visible light absorption and obvious photocatalytic activity due to their narrow band gap energy (Li et al. 2014). Silver nanoparticles absorb and scatter light with great efficiency. The strong interaction of silver nanoparticles with light occurs because the conduction electrons on the metal surface undergo a collective oscillation when excited by light at specific wavelengths. This oscillation is known as surface plasmon resonance (SPR) and causes the absorption and scattering intensity of silver nanoparticles to be much higher than non-plasmonic nanoparticles of the same size (Kushlyk et al. 2019). Also, the presence of silver with a higher oxidation and reduction potential than iron and cobalt can improve the efficiency of the catalyst in the process (Ziashahabi et al. 2019).

Composition with other compounds or functionalization by functional groups improves the performance of magnetic nanocatalysts. Polysaccharide and carbon compounds are materials that can be used as modifiers in the structure of these nanocatalysts. Polysaccharide compounds such as chitosan, CMC (Nasiri et al. 2022a, b) and MC (Golestani et al. 2022; Nasiri et al. 2022) are biodegradable, which due to the presence of functional groups such as amide, hydroxyl and carboxyl in their structure cause more interaction of the pollutant with the catalyst surface (Nasiri et al. 2019; Amirmahani et al. 2023). Carbon compounds such as graphene oxide and powdered activated carbon have also been considered in photocatalytic processes due to their high adsorption capacity, physicochemical stability, low toxicity and environment compatibility (Rajabi et al. 2022). The presence of functional groups such as hydroxyl, carboxyl and amine on the surface of carbon compounds creates a large number of active sites to increase electrocatalytic interaction and accelerate intermolecular conductivity. Studies reported that by modifying carbon composites with metal nanoparticles/oxide, the synthesized composite showed synergistic, antibacterial and higher degradability effects (Kichukova et al. 2022).

Since many countries use wastewater for irrigation in agriculture, therefore, lack of attention to their quality can cause severe environmental hazards. It should be noted that sometimes the incomplete oxidation of pollutants during the AOPs causes the formation of more toxic intermediate compounds; therefore, it is necessary to test the effluent toxicity using different organisms (Firoozi et al. 2023). Various organisms such as bacteria, invertebrates, algal species, plants and some fish have been used for the bioassay of toxins in wastewater. Bioassay based on plant growth includes the study of seed germination rate, number of leaves, measurement of stem and root length after exposing plants to different concentrations of wastewater (Karci 2014). This study was conducted with the aim of synthesizing AgCoFe₂O₄@Ch/AC as a new heterogeneous magnetic nanophotocatalyst for the CFTR degradation. The effect of pH, pollutant concentration, catalyst dose and time on the efficiency of the process was investigated and finally the effluent was evaluated for toxicity on the germination of watercress, tomato, lettuce and radish seeds.

Materials and methods

Chemicals and instrumentation

Silver nitrate ($AgNO_3$), cobalt nitrate hexahydrate ($Co(NO_3)_2.6H_2O$), iron(III) nitrate nonahydrate ($Fe(NO_3)_3.9H_2O$), chitosan, activated carbon, sodium hydroxide (NaOH) and hydrochloric acid (HCl) with laboratory grade (Merck Co, Germany) and ceftriaxone (98%) (Exir Co, Iran) were purchased. The solutions were prepared using distilled water. The pH of the solution was adjusted using NaOH and HCl 0.1 N.

Preparation of AgCoFe$_2$O$_4$@Ch/AC

AgCoFe$_2$O$_4$@Ch/AC was synthesized through a microwave-assisted co-precipitation method. First, $AgNO_3$ (0.338 g), $Co(NO_3)_2.6H_2O$ (1.89 g) and $Fe(NO_3)_3.9H_2O$ (8.06 g) were dissolved in 100 mL of distilled water. Chitosan (1 g) was added to the solution, and the suspension was stirred at room temperature. Then, NaOH was added drop-wise into the solution for 1 h until pH = 11, and finally 1 g of powdered active carbon was added to the suspension. The formed suspension was transferred to the microwave oven (SAMSUNG model, 2450 MHz, 450 W) for 15 min (3 × 5 min). After irradiation, the formed black precipitate was washed several times with distilled water and dried in an oven at 70 °C for 24 h (Nasiri et al. 2022c). The synthesis steps of AgCoFe$_2$O$_4$@Ch/AC are shown in Fig. 1.

Characterizations

The chemical structure and functional groups of the catalyst were identified by FTIR (AVATAR model, Termo). The morphology and physical structure of the catalyst, and the weight percentage of the catalyst elements, were investigated with FESM (MIRA III model, TESCAN) and EDX. Mapping analysis was used to abundance distribution the constituent elements of the catalyst surface as a point. Line scan analysis was also used to confirm the constituent elements of the catalyst linearly. XRD analysis (model PW1730, PHILIPS) was used to check the crystal structure and measure the size of AgCoFe$_2$O$_4$@Ch/AC crystals. The specific surface areas and pore size distributions of the catalyst, were measured by BET analysis (BELSORP MINI II model, BEL). Also, the magnetic power and optical activity of the catalyst were investigated with VSM (model MDKB, Kashan Kavir Magnet Company) and DRS (model DRS S-4100, SCINCO).

### Batch photodegradation experiments

All photocatalytic experiments were carried out in a Pyrex Photoreactor (Fig. 2) with a volume of 250 mL and in the presence of a UVC lamp (Osram model, 4W).

The effect of pH (3, 5, 7 and 9), CFTR concentration (5 mg/L, 10 mg/L, 15 mg/L, 20 mg/L and 25 mg/L), catalyst dose (0.02 g/L, 0.04 g/L, 0.08 g/L, 0.16 g/L, 0.24 g/L and 0.48 g/L), reaction time (5 min, 10 min, 15 min, 30 min and 60 min) and oxidant concentration (2 mM, 4 mM, 8 mM and 16 mM) on CFTR removal efficiency was evaluated. Then, the optimal conditions for antibiotic removal were determined. The residual concentration of CFTR was measured with a UV–Vis spectrophotometer (SHIMADZU, UV-1800) at a wavelength of $\lambda_{max} = 254$ nm, and the degradation rate is calculated (Eq. 1) as follows:
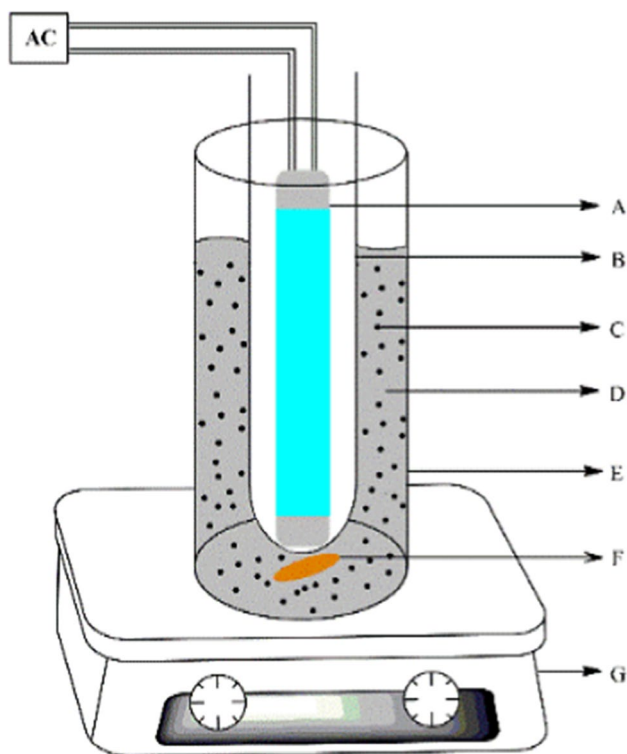
$$\text{Removal efficiency} = \frac{C_0 - C_t}{C_0} \times 100 \tag{1}$$

where C_0 and C_t are the CFTR concentration at initial and time t of the reaction, respectively. Limit of detection (LOD) and limit of quantification (LOQ) are calculated using Eqs. (2) and (3):

$$\frac{3.3 - S_b}{m} \tag{2}$$
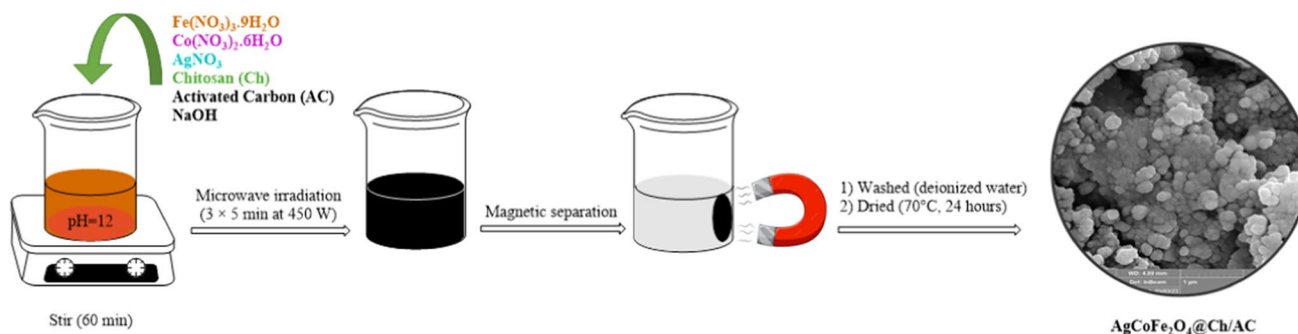
Fig. 1 Synthesis steps of heterogeneous magnetic AgCoFe$_2$O$_4$@Ch/AC nanophotocatalyst

Fig. 2 Schematic of the photoreactor (A: UV lamp, B: quartz glass, C: catalyst, D: solution containing ceftriaxone, E: Pyrex tank with a volume of 400 mL, F: magnet, G: stirrer)

$$LOQ = \frac{10 - S_b}{m} \tag{3}$$

where S_b and m are the standard deviation for blank and the slope of the calibration curve plot, respectively.

CFTR mineralization rate was also calculated by COD test according to Eq. (4):

$$\text{Mineralization efficiency} = \frac{COD_0 - COD_t}{COD_0} \times 100 \tag{4}$$

where COD_0 and COD_t are CFTR concentrations at initial and time t of the reaction, respectively.

To investigate the role of free radicals in CFTR degradation, ethanol (EtOH) was used as $^{\cdot}OH$ radical scavenger and chloroform ($CHCl_3$) as $O_2^{\cdot-}$ radical scavenger. CFTR removal efficiency was measured after adding 50 mM of radical scavengers under optimal conditions. The effect of different oxidants on the degradation efficiency of CFTR in optimal conditions was also investigated using hydrogen peroxide (H_2O_2), sulfate, persulfate (PS) and peroxymonosulfate (PMS) in concentrations of 2 mM, 4 mM, 8 mM and 16 mM.

In order to study the degradation rate of ceftriaxone from aqueous solution, *pseudo*-first order (Eq. 5) and Langmuir–Hinshelwood (Eq. 6) kinetic models were investigated.

$$Ln\frac{C_t}{C_0} = -K_{obs}.t \tag{5}$$

$$\frac{1}{K_{obs}} = \frac{1}{K_C \cdot K_{L-H}} + \frac{C_0}{K_C} \tag{6}$$

C_0 and Ct indicate the initial and final concentrations of CFTR (mg/L), respectively, K_{obs} (min^{-1}) is the reaction rate constant and t (min) refers to the reaction time. K_C (mg/L min) and K_{L-H} (L/mg) are reaction rate constant and adsorption equilibrium constant, respectively.

Determine the pH point of zero charge (pHzpc)

To calculate pHzpc, 50 mL of KCl solution (0.1 M) at pH of 2 g, 4 g, 6 g, 8 g, 10 g, 12 g and 0.01 g of AgCoFe$_2$O$_4$@Ch/AC was used. First, the initial pH of the solutions in the presence of catalyst was measured as initial pH (pH$_i$). Then, all the solutions at different pH were stirred for 24 h by rotator, and the final pH (pH$_f$) was also measured. Finally, ∆pH was measured and the intersection of the curve with the X axis was considered as pHzpc (Rajabi et al. 2022).

Reusability and chemical stability of AgCoFe$_2$O$_4$@Ch/AC

In order to determine the recovery rate of AgCoFe$_2$O$_4$@Ch/AC, the CFTR degradation was performed under optimal conditions and then the nanophotocatalyst was collected from the solution by a magnet. First, the nanophotocatalyst was washed with ethanol: distilled water (ratio 1:1) and then distilled water several times and finally dried in an oven at 70 °C (Yazdanpanah et al. 2023). AgCoFe$_2$O$_4$@Ch/AC was again used for antibiotic degradation, and this cycle was repeated four times.

Investigation of process efficiency on real wastewater

The efficiency of AgCoFe$_2$O$_4$@Ch/AC in removing CFTR from real wastewater was evaluated. For this purpose, the physical and chemical characteristics of wastewater were determined, then a certain concentration of antibiotic was added to it and transferred to the photoreactor. The residual concentration of CFTR in wastewater was measured using an HPLC (Azura model, Germany), on a C-18 column (4.6 × 150 mm, 5 μm), flow rate 1 mL/min, injection volume 20 μL and 2.4 min. The detector was set at 242 nm. The mobile phase consisted of sodium dihydrogen phosphate buffer and acetonitrile with a ratio of 35:65 (pH was adjusted to 2.8 using orthophosphoric acid).

Bioassay test

The toxicity of the effluent from the photoreactor was measured using the germination assay method by cress, lettuce, tomato and radish seeds. For this purpose, 48 sterile Petri dishes with filter paper were used. Thirty seeds of each plant sample were placed in each Petri dish.

Each of the seeds was irrigated separately with 5 mL of synthetic wastewater (5 mg CFTR/L), photoreactor effluent, raw wastewater and distilled water (blank) and kept at 25 °C and in the dark for 120 h. The average root length as well as the average number of germinated seeds in each sample were counted and compared with the control sample, and then the germination index (GI%) is calculated using (Eq. 7) (Rajabi et al. 2022).

$$\text{GI}(\%) = (\text{number of seeds} \times \text{total length of sample roots})/$$
$$(\text{number of seeds} \times \text{total length of control roots}) \times 100 \tag{7}$$

Results and discussion

Characterization of AgCoFe$_2$O$_4$@Ch/AC magnetic nano-heterogeneous photocatalyst

FESEM, analysis size distribution, EDS, mapping and line scan

The morphology and size of the synthesized nanophotocatalyst were investigated using FESEM analysis (Fig. 3a–b). FESEM images showed nanoparticles with *pseudo*-spherical shape, almost uniform, without aggregation and average particle size of about 80 nm. The histogram of particle size distribution showed that the average particles size is in the range of 80–100 nm (Fig. 3c). The analysis of the constituent elements of AgCoFe$_2$O$_4$@Ch/AC using EDS showed that the synthesized nanocatalyst contains carbon (45.68%), oxygen (22.42%), nitrogen (13.87%), iron (12.15%), cobalt (3.79%) and silver (2.09%) (Fig. 3d). Results of mapping analysis estimated that the elements C, N, O, Fe, Co and Ag had a homogeneous and uniform distribution on the surface of the nanophotocatalyst (Fig. 3e). Also, the line scan analysis, which was performed to check the type and quantity of constituent elements of the catalyst linearly (Fig. 3f), confirmed the presence of carbon, oxygen, nitrogen, iron, cobalt and silver with predictable weight values.

FTIR

Determination of the chemical structure and functional groups in the structure of chitosan, AgCoFe$_2$O$_4$ and AgCoFe$_2$O$_4$@Ch/AC was performed by FTIR analysis (Fig. 4). In the FTIR spectrum of chitosan, the peaks observed at wavelengths 1013 cm^{-1} and 1024 cm^{-1} correspond to free amine groups $-$NH$_2$, the peaks observed at the wavelengths of 1576 cm^{-1} and 1044 cm^{-1} correspond to the C–O band, the peak associated with the wavelength of 1421 cm^{-1} corresponds to the C–N band, and the peak observed at wavelength 3499 cm^{-1} is related to O–H (Majlesi and Daraei 2016; Nasiri et al. 2022; Kumar et al. 2016). In AgCoFe$_2$O$_4$, the peaks observed at 613 cm^{-1} and 937 cm^{-1} wavelengths are related to metal oxide bands in the ferrite structure of the nanocatalyst (Nasiri et al. 2022). In AgCoFe$_2$O$_4$@Ch/AC, the observed peaks at wavelengths of 618 cm^{-1} and 810 cm^{-1} are related to metal oxide in the tetrahedral structure (M$_{tetra}$–O) and metal oxide in the octahedral structure (M$_{octa}$–O) of the spinel structure of the nanocatalyst, respectively. Also, the peaks 1020 cm^{-1}, 1415 cm^{-1}, 1576 cm^{-1} and 3442 cm^{-1}, respectively, correspond to the functional groups NH$_2$, C–N, C–O and O–H in the structure of chitosan, which confirms the presence of chitosan in the final structure of the catalyst (Nasiri et al. 2022).

VSM

The magnetic strength of AgCoFe$_2$O$_4$@Ch/AC was checked using a vibrating sample magnetometer (VSM) (Fig. 5). According to the results, the values of saturation magnetism (Ms), residual magnetism (Mr) and magnetic coercive force (Hc) were 10.39 emu/g, 0.206 emu/g and 51 Oe, respectively. Also, the results showed that AgCoFe$_2$O$_4$@Ch/AC has high magnetic properties (Fig. 5b) and this magnetic property leads to faster and easier separation of the nanophotocatalyst from the reactor.

XRD

The crystal structure of AgCoFe$_2$O$_4$@Ch/AC was investigated using XRD analysis. According to Fig. 6a, chitosan structure was amorphous and showed a peak at $2\theta = 19.47°$. XRD peaks for AgCoFe$_2$O$_4$@Ch/AC were observed at $2\theta = 19.53°$, $35.56°$, $38.32°$, $43.70°$, $57.05°$ and $62.61°$. The XRD pattern confirmed that the structure of the nanocatalyst was magnetic heterogeneous in the ferrite phase (JCPDS 98-001-7262; 00-003-0864) and its crystal structure was still maintained after the composite with the amorphous phase of chitosan and active carbon. The average size of nanocatalyst crystals was calculated to be 5.49 nm using the Scherrer equation (Eq. 8).
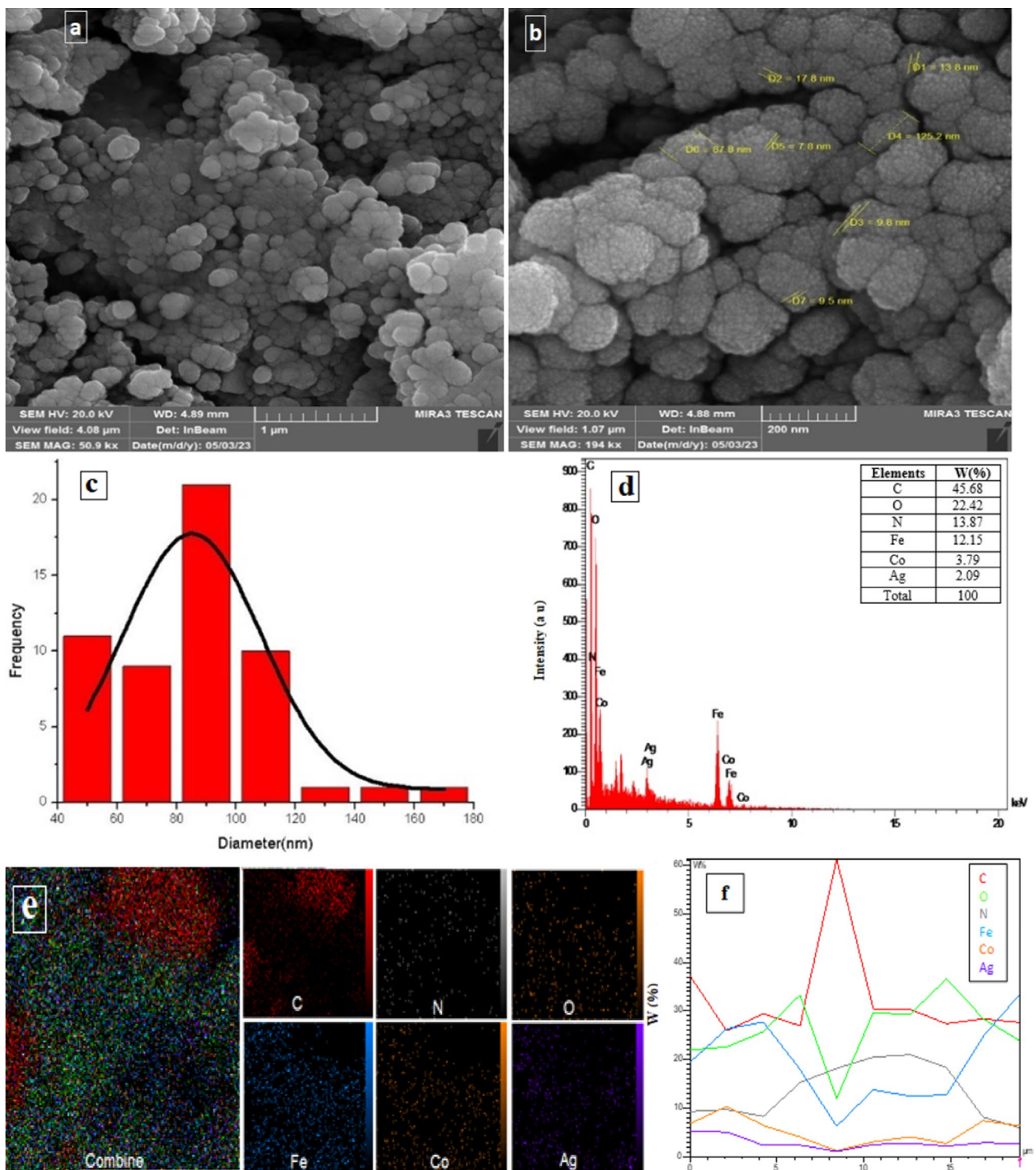
Fig. 3 FESEM (**a–b**), particle size distribution histogram (**c**), EDS (**d**), Mapping (**e**), Line scan (**f**) of AgCoFe$_2$O$_4$@Ch/AC

$$D = (K.\lambda)/(\beta.\cos\theta) \qquad (8)$$

where D, K, λ, β and θ represent the crystals size (nm), the shape factor (0.9), the X-ray wavelength (0.15406 nm), the

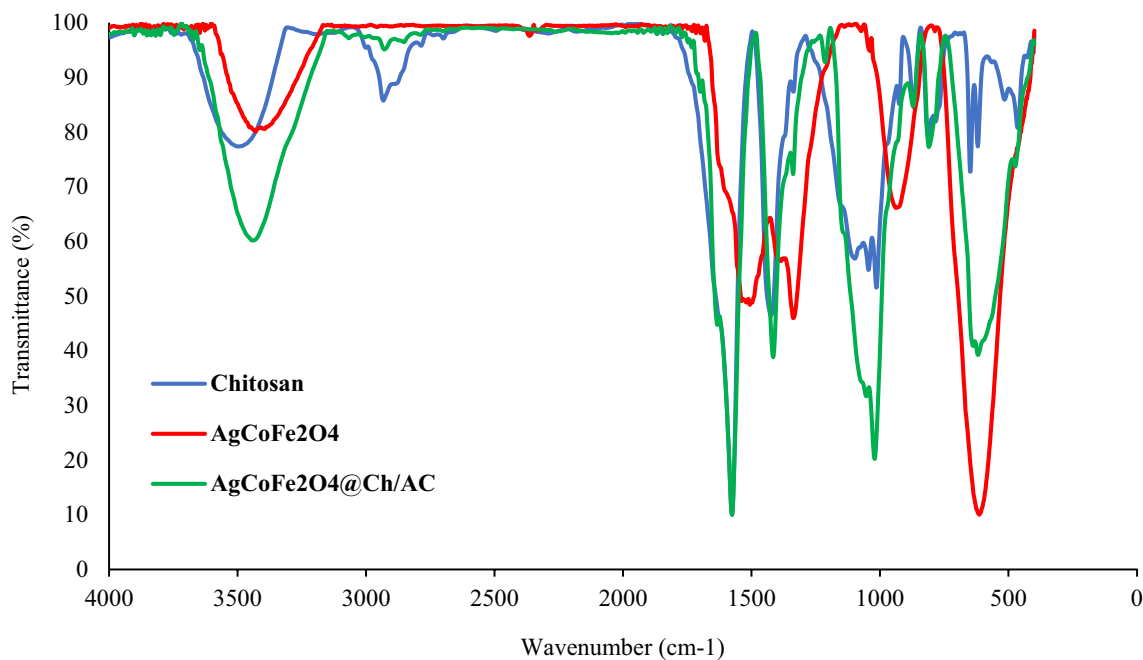peak width at half height (FWHM) and the Bragg angle, respectively.

Fig. 4 FTIR of chitosan (**a**), AgCoFe$_2$O$_4$ (**b**) and AgCoFe$_2$O$_4$@Ch/AC nanophotocatalyst (**c**)
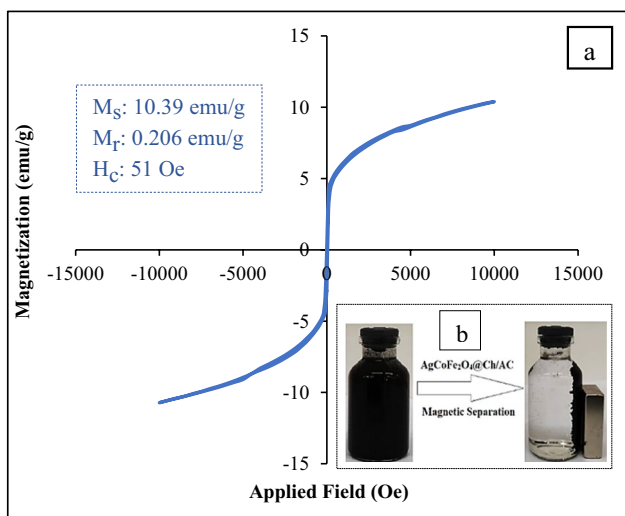

Fig. 5 VSM of AgCoFe$_2$O$_4$@Ch/AC (**a**), separation of nanophotocat-alyst in solution with magnet (**b**)

BET

Adsorption and desorption isotherm, BET surface area, *t*-plot and BJH of AgCoFe$_2$O$_4$@Ch/AC magnetic nanopho-tocatalyst are shown in Fig. 7. According to BET analysis, the specific surface area, average pore diameter, and total pore volume of the synthesized nanocatalyst were deter-mined to be 60.04 (m^2/g), 3.95 (nm), and 0.05 (cm^3/g),

respectively. Since the pore diameter has a high impact on the properties of porous materials, on this basis, the Inter-national Union of Pure and Applied Chemistry (IUPAC) has classified porous compounds into three categories: microporous (less than 2 nm), mesoporous (between 2 and 50 nm) and macroporous (more than 50 nm) Ariga et al. 2012. According to the obtained results, AgCoFe$_2$O$_4$@Ch/AC with a pore diameter of 3.95 nm is a mesoporous compound. Also, the high surface area of the nanocatalyst (60.04 m^2/g) causes more interaction with the pollutant and exposes more surface to UV rays to produce active radicals, which will increase the efficiency of the process.

DRS

UV–visible diffuse reflectance spectroscopy (UV–Vis DRS) was used to evaluate the optical properties of ferrite nanophotocatalyst and calculate the band gap (Fig. 8). The DRS results can provide useful information about photo-catalytic activity (Fard et al. 2019). Tauc equation (Eq. 9) was used to calculate the band gap (Alcaraz de la Osa et al. 2020).

$$\left[F(R_\infty)hv\right]^{1/2} = A\left(hv - E_g\right) \tag{9}$$

where $F(R_\infty)$, hv, A and E_g are Kubelka–Munk function, light photon energy, constant value and band gap, respec-tively. Figure 8a shows the obtained results from DRS

Fig. 6 XRD pattern of chitosan (**a**) and AgCoFe$_2$O$_4$@Ch/AC (**b**)
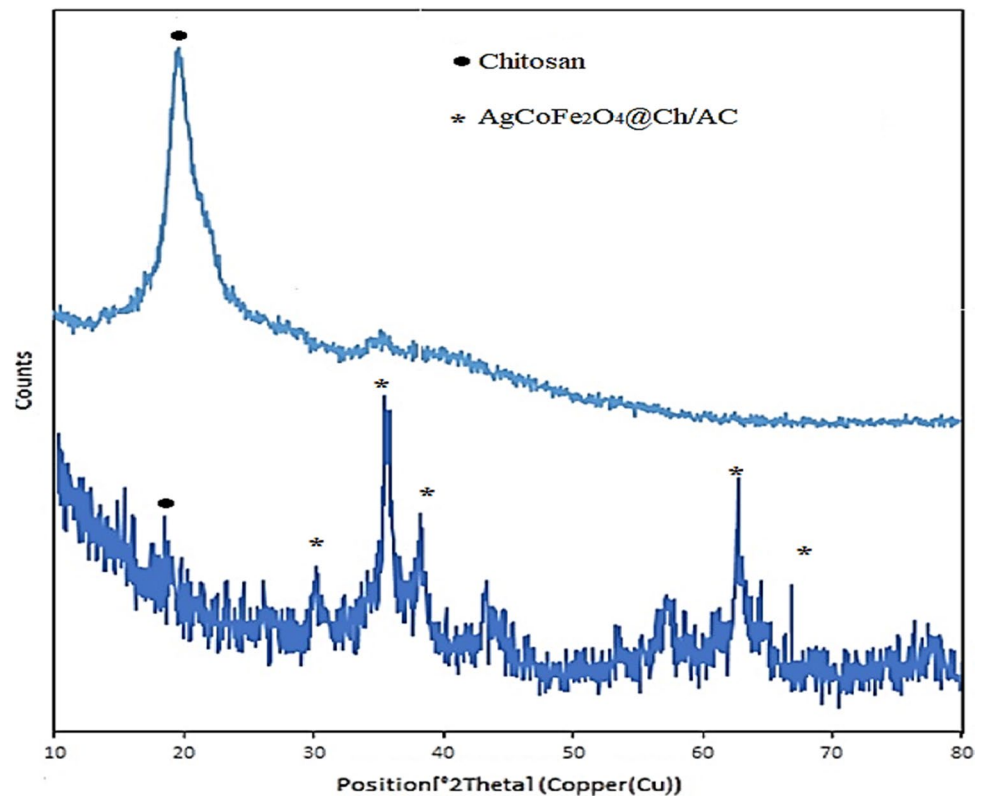
analysis of AgCoFe$_2$O$_4$@Ch/AC, which was used to calculate the bandgap value of the catalyst ($E_g = 3.1$ eV). The results are shown in Fig. 8b.

Optimization parameters of CFTR photodegradation

Since pH is one of the most important factors in photocatalytic processes, its effect in the ranges of 3, 5, 7 and 9 in the CFTR removal with AgCoFe$_2$O$_4$@Ch/AC was investigated (Fig. 9a). According to the results, the highest (82.4%) and lowest (5.82%) removal efficiency were observed at pH = 3 and pH = 9, respectively. Considering that the solubility of iron is higher at low pH, therefore, acidic conditions in the reactor can lead to increased degradation of CFTR (Kamranifar et al. 2019). pH$_{zpc}$ indicates the surface charge of the catalyst at different pHs. As shown in Fig. 9b, the pH$_{zpc}$ of the catalyst was 7, which means that at pHs higher than pH$_{zpc}$, the surface charge of the AgCoFe$_2$O$_4$@Ch/AC in aqueous solution is negative, and at lower pHs, its surface charge is positive (Firoozi et al. 2023). Because the highest removal efficiency of CFTR was obtained at a pH lower than pH$_{zpc}$, therefore the surface charge of the catalyst is positive. pKa is considered as one of the basic factors on the protonation of pollutant compounds in aqueous solutions. Since the pKa value for CFTR has been found to be 3, 3.2 and 4.1 (Karungamye et al. 2022), therefore, this antibiotic is more present in cationic form in acidic pHs and in

anionic form in alkaline pHs. Ceftriaxone is a hydrophobic organic compound and tends to separate from the aqueous phase and adsorb on the surface of the solid catalyst under lyophobic forces. With pollutant adsorption on the catalyst surface, the destructive effect of the catalyst increases. On the other hand, under alkaline conditions, CFTR tends to anionic form and the surface charge of the catalyst is also negative. Therefore, in alkaline pHs, the electrostatic repulsion force between the surface of the catalyst and the antibiotic reduces the degradation rate of CFTR (Takdastan et al. 2020). Takdestan et al. in 2020 also reported similar results in the photocatalytic degradation of CFT at acidic pHs (Takdastan et al. 2020).

The effect of different nanocatalyst doses (0.02–0.48 g/L) on ceftriaxone removal was investigated (Fig. 9c). The results showed that 98.8% removal of ceftriaxone was observed at a dose of 0.24 g/L and 60.4% degradation was observed at a dose of 0.02 g/L. Also, by increasing the catalyst dose from 0.24 to 0.48 g/L, the removal efficiency of CFTR decreased to 90.3%. According to the obtained results, the optimal dose of catalyst was considered to be 0.24 g/L of catalyst. The increase in the removal efficiency by increasing the catalyst dose can be caused by the production of more free radicals, the increase in active sites on the surface of the catalyst, and also the higher absorption of UV photons (Daraei et al. 2023). On the other hand, increasing the catalyst dosage increased the turbidity in the solution

Fig. 7 Adsorption and desorption isotherm (**a**), BET (**b**), t-plot (**c**) and BJH (**d**) of AgCoFe$_2$O$_4$@Ch/AC
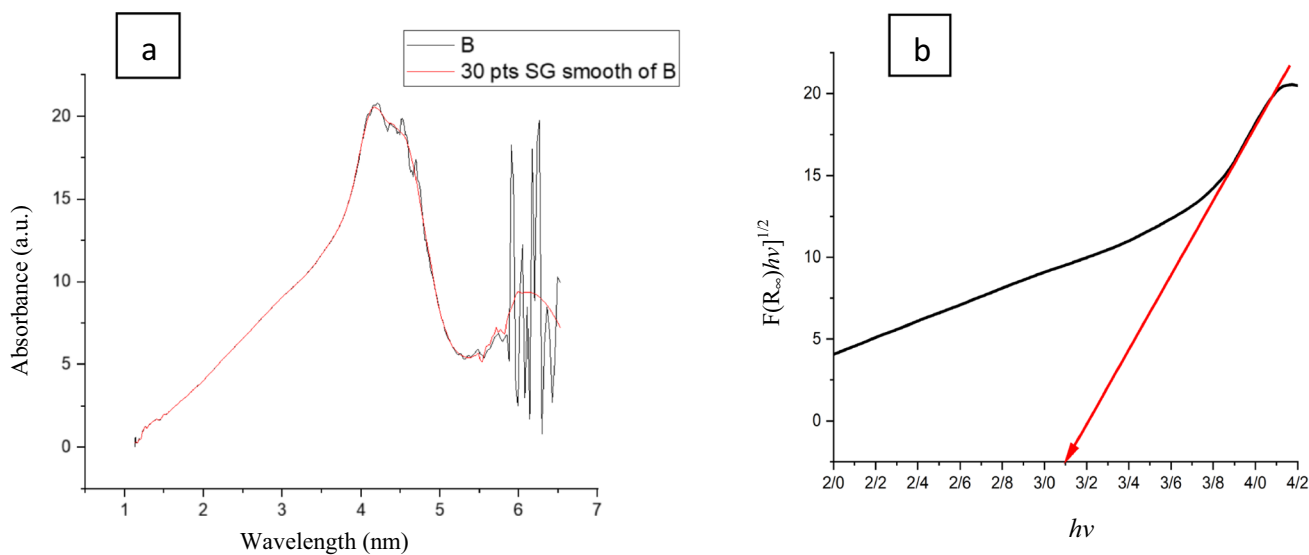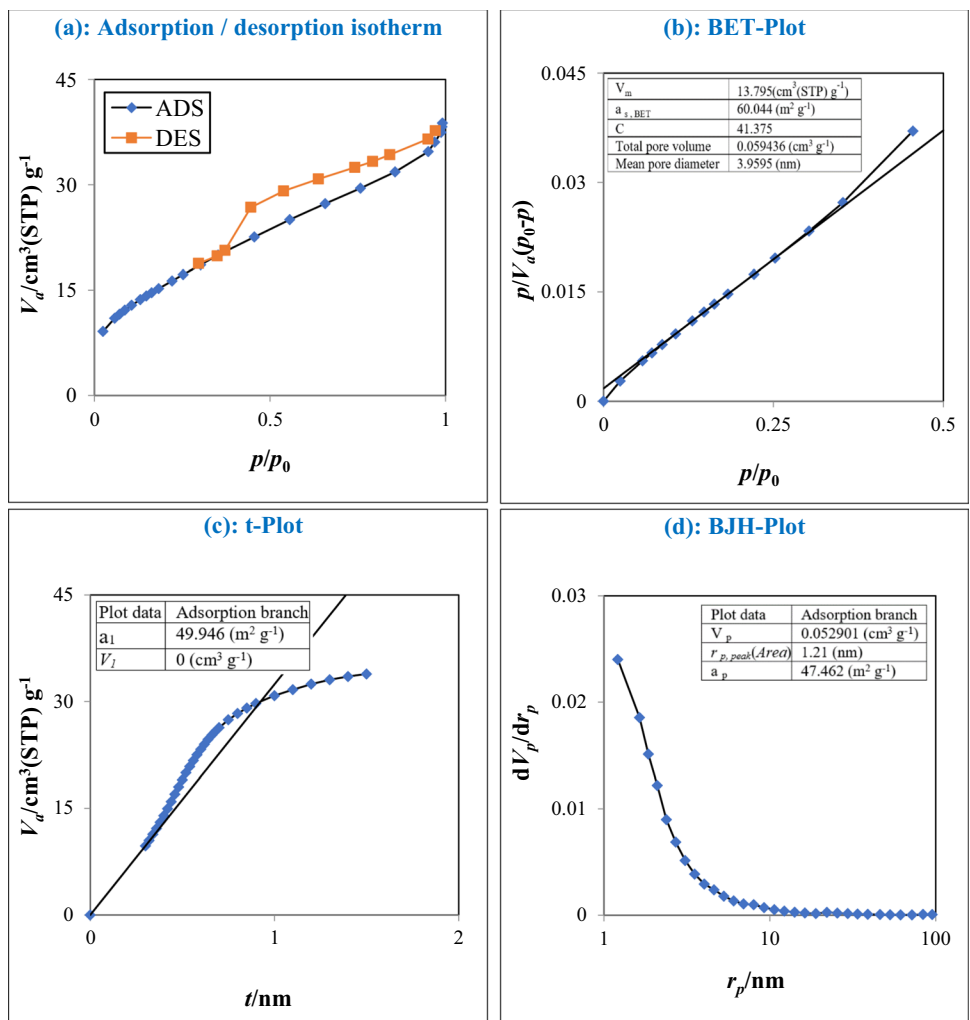
Fig. 8 DRS analysis (**a**) band gap calculation (**b**) of AgCoFe$_2$O$_4$@Ch/AC
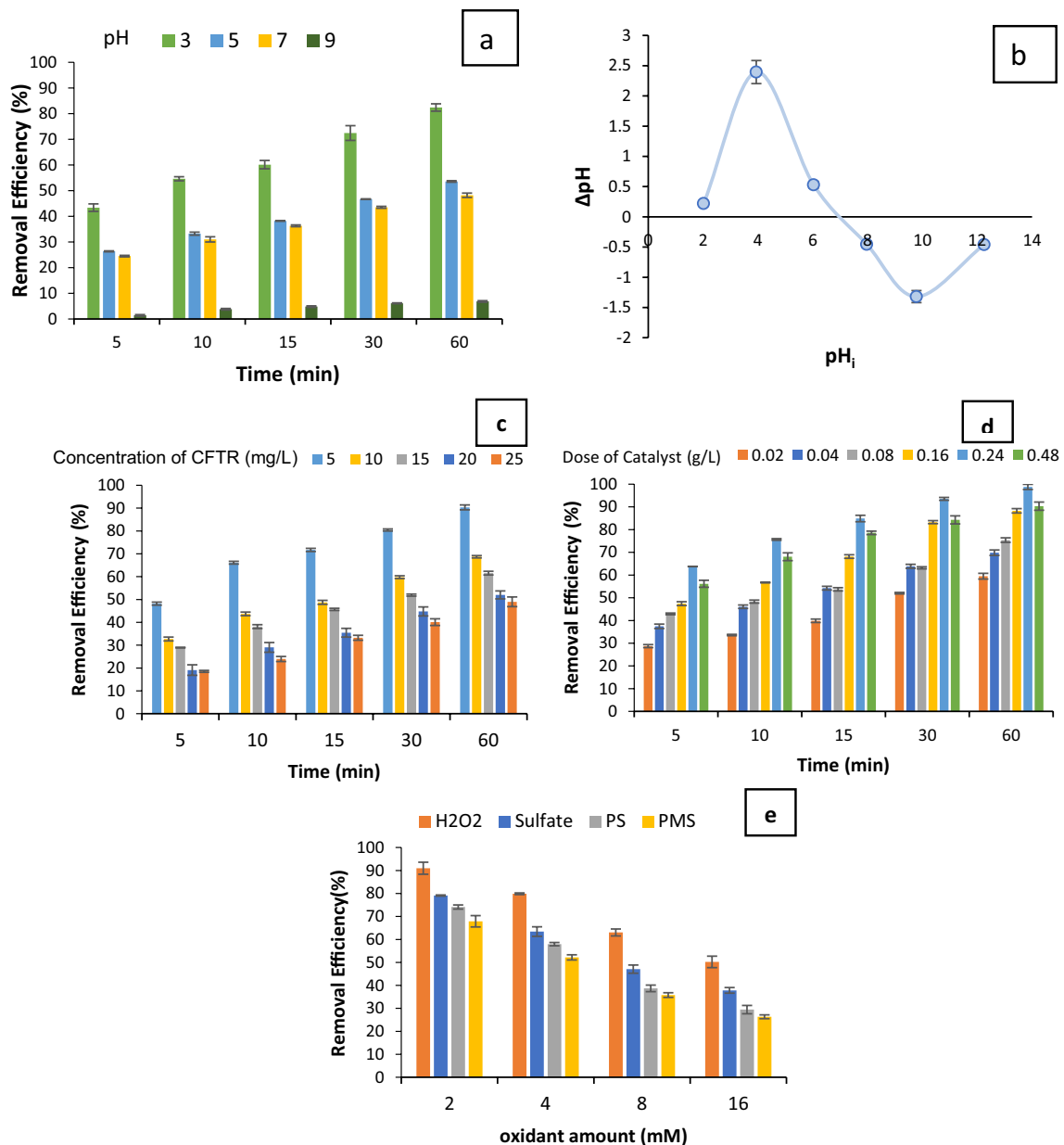
Fig. 9 Effect of pH (**a**), pH$_{zpc}$ (**b**), catalyst dose (**c**), CFTR concentration (**d**), oxidants concentration (**e**) in CFTR removal (pH = 3, catalyst = 0.24 g/L, C = 5 mg /L, T = 60 min)

due to the ferritic structure of the catalyst. Turbidity reduces the penetration of UV radiation in the solution and on the surface of the catalyst, and as a result, it leads to a reduction in the production of active radicals. Nasiri et al. in 2019 have achieved similar results in the removal of ciprofloxacin during the photocatalytic processes, and by increasing the amount of catalyst, the removal efficiency was decreased (Nasiri et al. 2019).

The effect of initial ceftriaxone concentrations (5 mg/L, 10 mg/L, 15 mg/L, 20 mg/L and 25 mg/L) on the nanophotocatalytic removal process was investigated. According to

Fig. 9d, the removal efficiency of CFTR decreased from 90.3 to 49% by increasing its concentration from 5 to 25 mg/L. This decrease in removal efficiency can be due to the increase in the production of intermediates at high CFTR concentrations and their competition to occupy the active sites of the nanocatalyst (Takdastan et al. 2020). In addition, in higher concentrations of CFTR, the number of active radicals is not enough to decompose significant amounts of the pollutant. Other reasons for the decrease in efficiency at high CFTR concentrations are the decrease in the penetration of UV photons in the solution and as a result the decrease in

the production of electron/hole pairs (e^-/h^+) on the surface of the catalyst and active radicals (Khorsandi et al. 2019). In the study on the photocatalytic degradation of ceftriaxone by Khorsandi et al., similar results were obtained, and at high ceftriaxone concentrations, the removal efficiency decreased (Khorsandi et al. 2019).

The effect of concentration of some oxidants (such as H_2O_2, sulfate, PS and PMS) on the CFTR degradation in the presence of $AgCoFe_2O_4@Ch/AC$ was investigated in 60 min. As shown in Fig. 9e, the removal efficiency of ceftriaxone decreased with increasing dose of oxidants from 2 to 16 mM. The reduction in CFTR degradation in high amounts of oxidants can be due to the fact that oxidants in high concentrations act as a scavenger of free radicals such as ˙OH (López-Peñalver et al. 2010). Also, the decrease in efficiency in high concentrations of sulfate, persulfate and monosulfate can be due to the absorption of active radicals by mineral ions (Rajabi et al. 2022). Among the studied oxidants, hydrogen peroxide showed more oxidizing power (91%). However, in the absence of oxidants, the removal efficiency of CFTR in optimal conditions was obtained 98.8%. According to the reduction in CFTR degradation in

the presence of oxidants, these compounds had an inhibitory role in the nanophotocatalytic process, which could be due to the following reasons. Anions produced due to the dissolution of oxidants can occupy the active sites on the catalyst surface and reduce the nanophotocatalyst performance (Daraei et al. 2023). Some mineral ions absorb the generated active radicals and reduce the degradation efficiency. Some inorganic anions can increase the pH of the solution and reduce the efficiency of the reactor (Lu et al. 2020).

Kinetic study of ceftriaxone photodegradation

Pseudo-first-order kinetics data on the CFTR degradation by $AgCoFe_2O_4@Ch/AC$ are presented in Table 1.

By plotting the $1/K_{obs}$ curve against the CFTR concentration (Fig. 10a), a linear equation was obtained, which was used to calculate K_C and $K_{L–H}$. The amount of K_C and $K_{L–H}$ was calculated as 0.23 mg/L min and 0.168 L/mg, respectively. The results showed that the CFTR degradation follows *pseudo*-first-order and Langmuir–Hinshelwood kinetics ($R^2 = 0.928$), and the photocatalytic degradation of ceftriaxone depends on the CFTR concentration (Yang et al. 2023). Absorption intensity changes in CFTR degradation under optimal conditions and different irradiations times were investigated (Fig. 10b), and the main peak of ceftriaxone was obtained at $\lambda_{max} = 254$ nm. According to Fig. 10b, with the increase in time from 5 to 60 min, the intensity of absorption peak decreased due to the decrease in CFTR concentration. Also, LOD and LOQ were obtained as 0.052 mg/L and 0.2272 mg/L, respectively, which indicated that the data obtained in the present study were within the limit of spectrophotometer detection. Previous similar results of photocatalytic studies for the removal of ceftriaxone from

Table 1 *Pseudo*-first-order kinetic parameters in ceftriaxone degradation by $AgCoFe_2O_4@Ch/AC$

C_0(mg/L)	R^2	K_{obs}(1/min)	$t_{1/2}$(min)	Line Eq.
5	0.95	0.0280	24.75	$y = -0.028 \times + 0.8840$
10	0.93	0.0131	52.90	$y = -0.0131 \times + 1.8723$
15	0.92	0.0102	67.94	$y = -0.0102 \times + 2.3261$
20	0.89	0.0087	79.65	$y = -0.0087 \times + 2.7407$
25	0.91	0.0081	85.55	$y = -0.0081 \times + 2.9982$
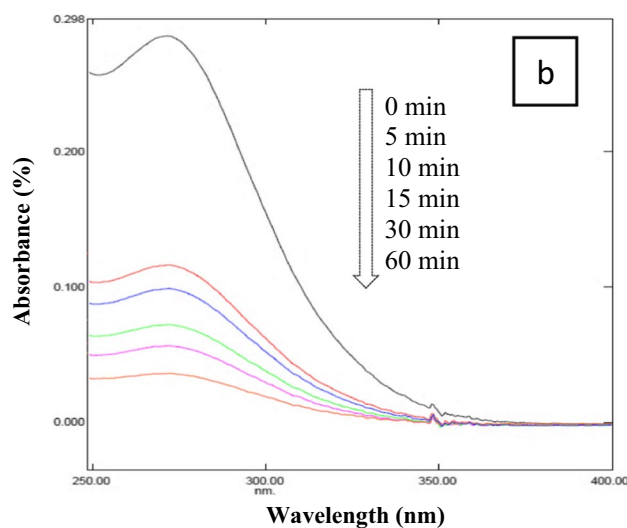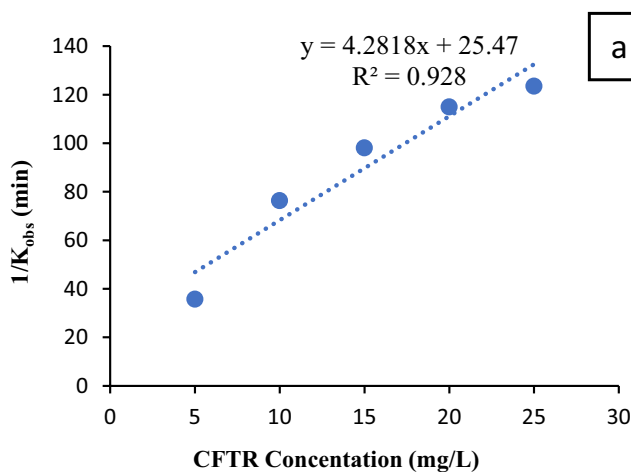
Fig. 10 Langmuir–Hinshelwood kinetic diagram (**a**), spectrum of CFTR absorption intensity changes in 5 to 60 min (**b**) (pH = 3, catalyst = 0.24 g/L, C = 5 mg/L)
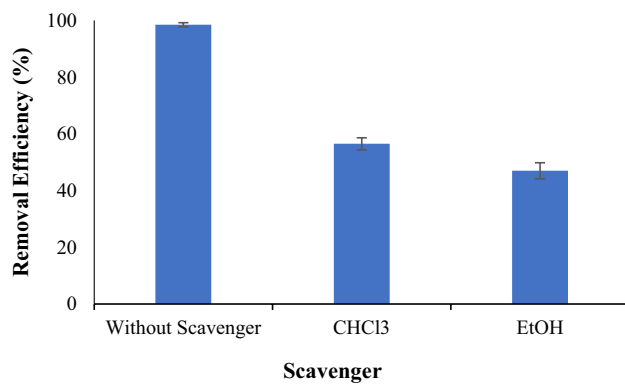
Fig. 11 The effect of $CHCl_3$ and EtOH as radical scavengers in CFTR removal (pH = 3, catalyst = 0.24 g/L, $C_{ceftriaxone}$ = 5 mg/L, T = 60 min, $C_{scavenger}$ = 50 mM)

aqueous solutions showed that the kinetics of the photocatalytic removal of ceftriaxone follows *pseudo*-first-order and Langmuir–Hinshelwood kinetic models (Khorsandi et al. 2019).

Effect of radical scavengers on ceftriaxone photodegradation

To investigate the role of different free radicals in the degradation of CFTR, scavengers of ethanol (EtOH) were used as scavengers of $^{\bullet}OH$ and chloroform ($CHCl_3$) as scavengers of $O_2^{-\bullet}$. The results showed (Fig. 11) that by adding 50 mM of chloroform and ethanol under optimal conditions, the removal efficiency decreased from 98.8 to 58% and 49%, respectively. Considering the more reduction in efficiency in the absence of hydroxyl radical, therefore, $^{\cdot}OH$ radicals play a more important role in CFTR degradation (Khorsandi et al. 2019). During a photocatalytic removal of ceftriaxone, Khorasani et al. reported similar results regarding the effect of hydroxyl radicals in the ceftriaxone degradation (Khorsandi et al. 2019).

Comparison of peroxides and catalytic performance

Ceftriaxone degradation rate was investigated in different photocatalytic, photolysis and adsorption processes. As shown in Fig. 12, the highest removal efficiency of CFTR in the photocatalytic process was obtained with $AgCoFe_2O_4@$ Ch/AC (92.6%). Also, the lowest efficiency was related to the UV/Ch process (3.1%). The high degradation of ceftriaxone in the UV/$AgCoFe_2O_4@$Ch/AC process can be due to the production of more active radicals in the presence of the catalyst and UV rays. Also, the comparison of $AgCoFe_2O_4@$ Ch/AC and $CoFe_2O_4@$Ch/AC in CFTR removal showed that the presence of Ag in the catalyst structure improves the AOP performance due to its higher oxidation–reduction
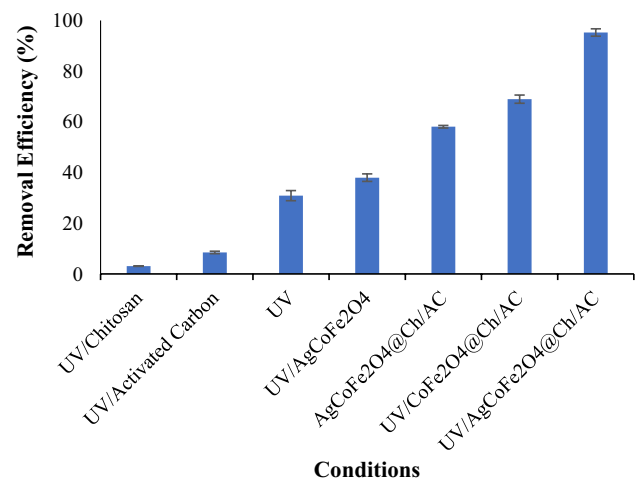
Fig. 12 Comparison of different processes in CFTR removal (pH = 3, catalyst = 0.24 g/L, C = 5 mg/L, T = 60 min)

potential (0.8 eV) compared to Co (−0.28 eV) and Fe (−0.036 eV) (Ziashahabi et al. 2019). In the photocatalytic process, silver, cobalt and iron electrons in the catalyst structure can activate dissolved oxygen to produce superoxide anion radicals, and the holes created on the $AgCoFe_2O_4@$ Ch/AC surface can also convert water into hydroxyl radicals. Active species (superoxide anion radicals and hydroxyl radicals) can react with CFTR adsorbed on catalyst and lead to its degradation (Chen et al. 2016). On the other hand, the absence of chitosan and active carbon in the nanophotocatalyst structure can lead to a decrease in the surface adsorption power of the catalyst and as a result, a decrease in the interaction between the pollutant and the catalyst (Kichukova et al. 2022). Also, the significant reduction of CFTR removal in UV/AC and UV/Ch processes can be due to the increase in turbidity, decrease in UV penetration in the solution and the absence of the ferrite part to produce radicals.

Mineralization study

COD removal was evaluated as an indicator to investigate the CFTR mineralization. COD removal in synthetic wastewater and real wastewater in the presence of $AgCoFe_2O_4@$ Ch/AC and under optimal conditions was obtained 85% and 78%, respectively. The results showed the high ability of heterogeneous magnetic nanophotocatalyst in antibiotic mineralization. In 2016, Shokri et al. investigated pollutant mineralization using COD removal during the photocatalytic process of ceftriaxone degradation and reported similar results (Shokri et al. 2016).
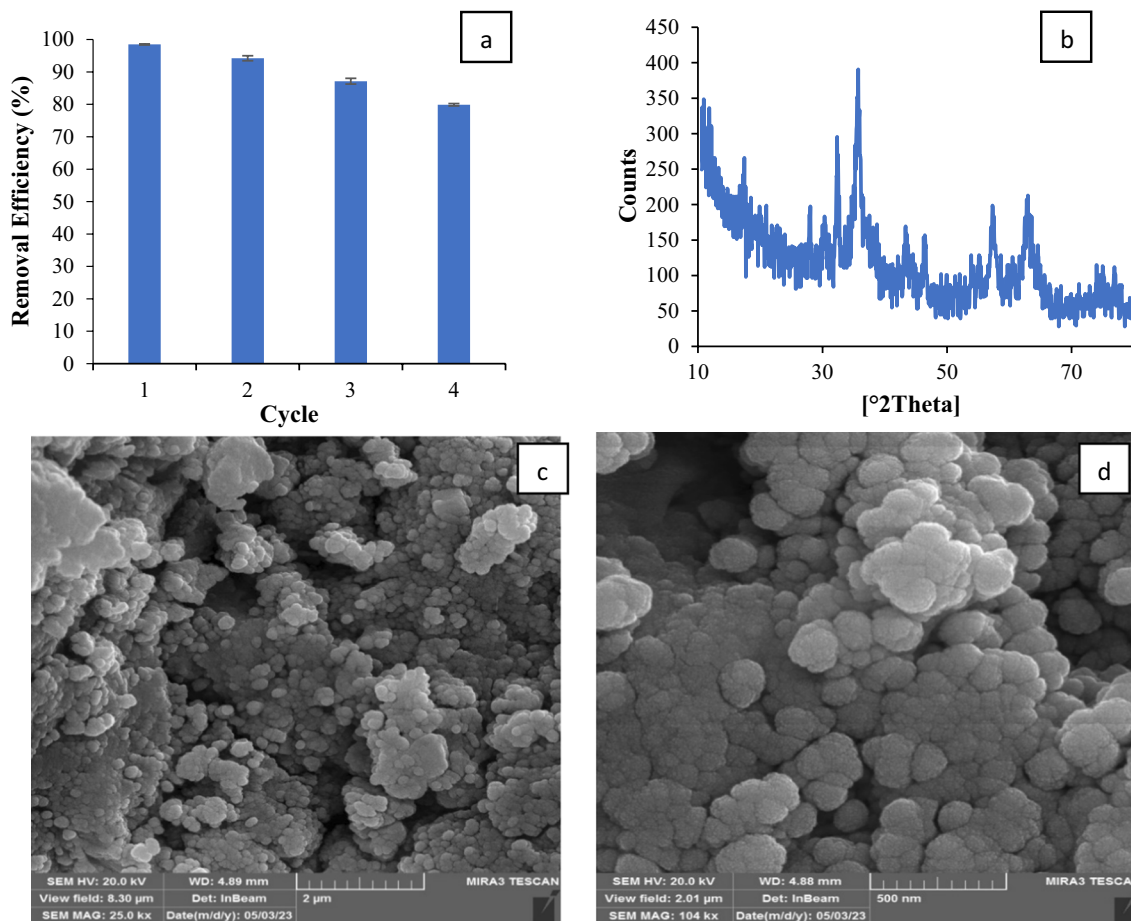
Table 2 Physicochemical properties of real wastewater samples

Entry	Parameters	Amount
1	pH	7.6
2	EC (mho/cm)	1.88
3	(mg/L)	1128
4	TSS (mg/L)	0.1 >
5	BOD (mg/L)	65
6	COD (mg/L)	120
7	SO_4 (mg/L)	350
8	TKN (mg/L)	< 0.1
9	NO_3 (mg/L)	25.1
10	PO_4 (mg/L)	14.4
11	CEFT (mg/L)	4.86

Under optimal conditions, the photocatalytic process was applied to remove ceftriaxone in real wastewater, and the removal efficiency was 79.01%. This decrease in efficiency can be due to the presence of interfering factors such as cations and anions in the real wastewater sample, which play an inhibitory role in the action of oxidizer radicals. Sulfate, nitrate and phosphate anions in real wastewater can react with hydroxyl radicals and reduce the number of oxidizing radicals in the solution. These anions can also reduce the production of hydroxyl radicals in the reaction medium for the oxidation of ceftriaxone by absorbing UV rays (Moussavi et al. 2018). In addition, these interfering factors can occupy the active sites of the catalyst and reduce the efficiency of the process. In the study of ciprofloxacin photocatalytic degradation, Nasiri et al. reported similar results on real wastewater (Nasiri et al. 2019).

Investigation of process efficiency on real wastewater

The efficiency of the photocatalytic process was also investigated on a real wastewater sample. The results of the physicochemical quality analysis of wastewater are reported in Table 2.

Fig. 13 CFTR removal efficiency (**a**), XRD (**b**), FESEM (**c–d**) of AgCoFe$_2$O$_4$@Ch/AC after four regeneration stages

Reusability and chemical stability of AgCoFe$_2$O$_4$@Ch/AC

Chemical stability and reusability of the synthesized nano-photocatalyst is important from the environmental and economic aspects. For this purpose, the catalyst was collected using a magnet, washed, dried and used for the next cycle. As shown in Fig. 13a, the nanocatalyst was able to remove 80.16% of ceftriaxone after four regeneration cycles, which indicates the high efficiency of the catalyst. This slight decrease in efficiency can be caused by the occupation of the active sites of the catalyst by precursors and intermediates (Rajabi et al. 2022).

The leaching rate, morphology and crystal structure of the catalyst were evaluated in order to determine the chemical stability of the catalyst after four regeneration cycles. The leaching rate of the catalyst was checked by measuring the concentration of silver, cobalt and iron in the effluent. The results showed that the concentration of these elements in the effluent for Ag, Co and Fe was 0.015 mg/L, 0.061 mg/L and 0.011 mg/L respectively, which was very insignificant. Also, the concentration of these elements in the process effluent according to the EPA and WHO standards were below the permissible limit (Ag = 0.1 mg/L, Co = 2.5 mg/L and Fe = 2 mg/L) in the wastewater (Nasiri et al. 2022c; Long and Martin 1989).

The results of XRD analysis after four regeneration cycles of nanophotocatalyst (Fig. 13b) showed that there was no change in the crystal structure of the catalyst and sharp peaks related to the ferrite phase were visible. Figure 13c–d shows that after four catalyst regeneration cycles, its morphology, shape and physical structure were still maintained. These results show the regeneration and high chemical stability of AgCoFe$_2$O$_4$@Ch/AC during the photocatalytic process.

Photodegradation mechanism

The degradation mechanism of CFTR by AgCoFe$_2$O$_4$@Ch/AC is shown in Fig. 14. UV radiation on the valence layer leads to the excitation of electrons (e$^-$), their transfer to the conductive layer and the generation of holes (h$^+$) in the valence layer. The e$^-$/h$^+$ pair leads to the production of hydroxyl and superoxide radicals during the following reactions (Daraei et al. 2023). Also, the conversion of silver, cobalt and iron in the solution to multivalent forms due to oxidation and reduction helps to produce more active radicals (Rajabi et al. 2022). The radicals produced in the presence of the catalyst and in the photoreactor lead to further degradation of CFTR to less dangerous compounds (Eq. 10–22).
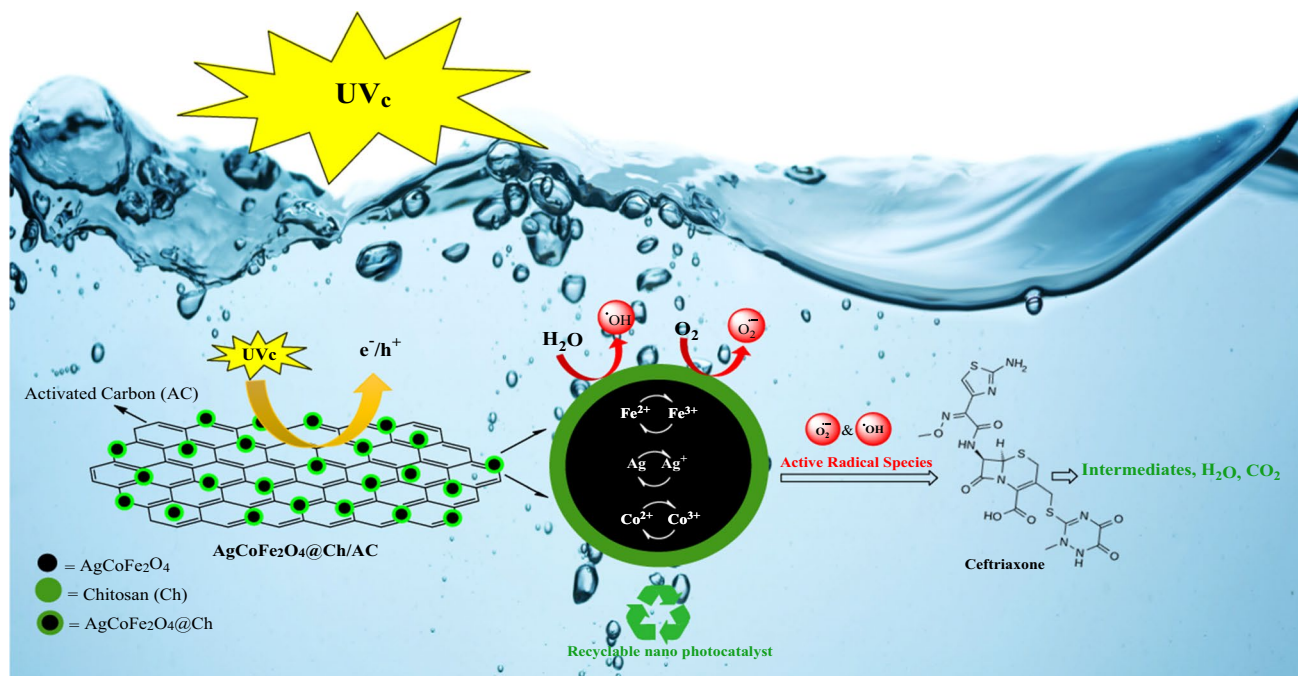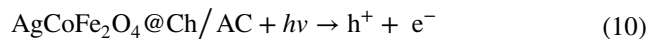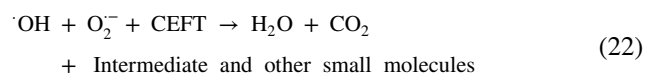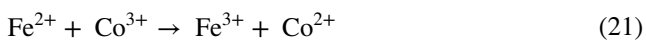
$$AgCoFe_2O_4@Ch/AC + hv \rightarrow h^+ + e^- \tag{10}$$

$$h^+ + H_2O \rightarrow h^+ + {}^\cdot OH \tag{11}$$

$$e^- + O_2 + h^+ \rightarrow {}^\cdot OH \tag{12}$$

Fig. 14 Ceftriaxone degradation mechanism by AgCoFe$_2$O$_4$@Ch/AC nanophotocatalyst

$$e^- + O_2 \rightarrow O_2^{\cdot-} \tag{13}$$

$$2H^+ + 2O_2^{\cdot-} \rightarrow O_2 + H_2O_2 \tag{14}$$

$$H_2O_2 \rightarrow 2^{\cdot}OH \tag{15}$$

$$Fe^{3+} + H_2O \rightarrow Fe^{2+} + ^{\cdot}OH + H^+ \tag{16}$$

$$Fe^{2+} + O_2 \rightarrow Fe^{3+} + O_2^{\cdot-} \tag{17}$$

$$Ag \rightarrow Ag^+ + e^- \tag{18}$$

$$Co^{3+} + e^- \rightarrow Co^{2+} \tag{19}$$

$$Co^{2+} + H_2O_2 + H^+ \rightarrow Co^{3+} + H_2O + ^{\cdot}OH \tag{20}$$

$$Fe^{2+} + Co^{3+} \rightarrow Fe^{3+} + Co^{2+} \tag{21}$$

$$^{\cdot}OH + O_2^{\cdot-} + CEFT \rightarrow H_2O + CO_2 \\ + \text{ Intermediate and other small molecules} \tag{22}$$
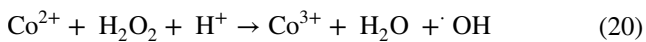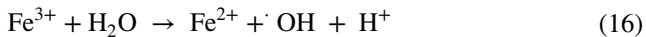
Photocatalytic performance of AgCoFe$_2$O$_4$@Ch/AC *vs* other photocatalysts

The photocatalytic removal of CFTR in the presence of AgCoFe$_2$O$_4$@Ch/AC was compared with some studies conducted in the photocatalytic removal of pharmaceutical compounds (Table 3).

Comparison of AgCoFe$_2$O$_4$@Ch/AC efficiency in CFTR removal with the results of other studies showed that the present process has removed the antibiotic with a higher efficiency in shorter time and lower catalyst dose. The mineralization rate (85%) of the CFTR was higher compared to other studies. Also, the synthesized nanophotocatalyst was able to remove 80.16% of the antibiotic after 4 cycles of regeneration, which leads to AgCoFe$_2$O$_4$@Ch/AC being prioritized over other catalysts.

Germination tests

Treated effluent obtained under optimal conditions, synthetic wastewater, and real wastewater was used in the toxicity tests on the germination of watercress, radish, tomato and lettuce seeds. As shown in Fig. 15a, the germination rate in watercress and tomato seeds irrigated with treated effluent

Table 3 Comparison of efficiency of AgCoFe$_2$O$_4$@Ch/AC in antibiotic removal with other studies

Drug (Refs.)	Photocatalyst	pH	C_0 (mg/L)	Time (min)	Dose (g/L)	Removal efficiency (%)	Mineralization (%)	Removal efficiency (real wastewater) (%)	Cycle	Removal efficiency (reuse) (%)
Gemfibrozil Sayadi et al. (2021)	Ag-CuFe$_2$O$_4$@WO$_3$	5	5	150	0.2	81	–	–	5	72.64
Tamoxifen Sayadi et al. (2021)	Ag-CuFe$_2$O$_4$@WO$_3$	5	5	150	0.2	83	–	–	5	68.25
Acetaminophen Ramasamy et al. (2021)	Ag-ZnO	8.5	5	120	1	90.8	60	–	–	–
Metronidazole Tamaddon et al. (2020a)	ZnFe$_2$O$_4$@MC	7	5	100	0.3	92.65	77.87	71.12	6	85.58
Ciprofloxacin Tamaddon et al. (2020b)	CuFe$_2$O$_4$@MC	7	3	90	0.2	80.74	68.26	72.87	4	73.78
Ciprofloxacin Malakootian et al. (2019)	ZnFe$_2$O$_4$@CMC	7	5	100	0.3	87	75	79	5	80
Levofloxacin Sharma et al. (2018)	TiO$_2$/Carbon-dots	6	10	90	0.25	96	53.4	–	–	–
Sulfamethoxazole Kim and Kan (2016)	Biochar/TiO$_2$	4	10	180	0.5	74	66	–	–	–
Ceftriaxone (This work)	AgCoFe$_2$O$_4$@Ch/AC	3	5	60	0.24	98.8	85	79.01	4	80.16
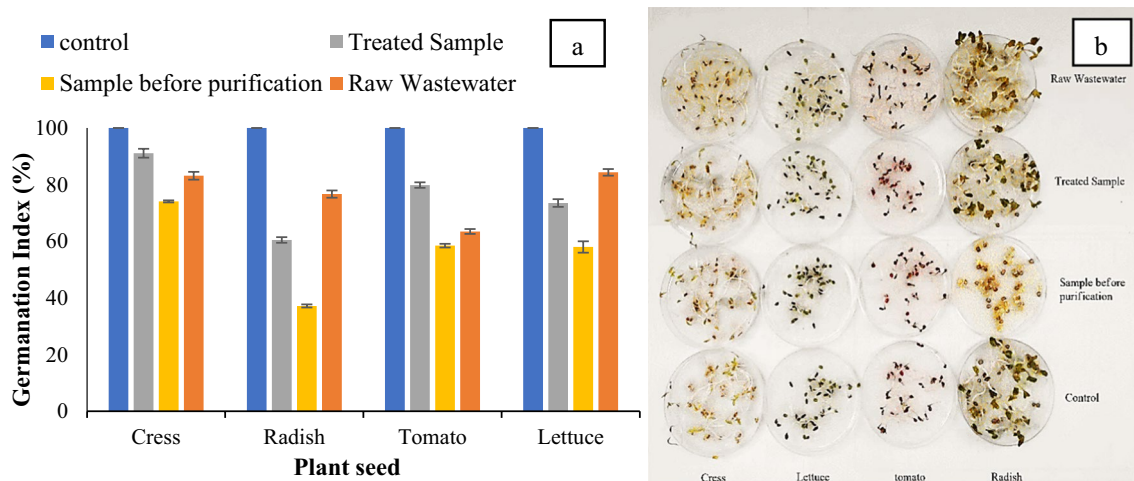
Fig. 15 Germination index of watercress, radish, tomato and lettuce seeds (**a**), germination rate of watercress, radish, tomato and lettuce seeds after 5 days of incubation (**b**)

is higher than the real wastewater sample and close to the control sample. On the other hand, the germination rate of lettuce and radish seeds in raw wastewater was higher than treated wastewater. However, all seeds reacted to wastewater containing ceftriaxone and showed a significant reduction in their growth. The highest sensitivity to ceftriaxone was related to radish seeds. Therefore, ceftriaxone can be environmentally dangerous and have an adverse effect on plant growth. However, the results of CFTR degradation with AgCoFe$_2$O$_4$@Ch/AC showed that all seeds had an increase in GI index, which indicates the high efficiency of this process in CFTR removal from aqueous environments (Priac et al. 2017). In a similar study, Priac et al. concluded that the seed germination rate depends on the culture medium and the sensitivity of the seeds (Priac et al. 2017).

Conclusion

In present study, an economic and green heterogeneous magnetic nanophotocatalyst AgCoFe$_2$O$_4$@Ch/AC was synthesized and its efficiency was evaluated in the CFTR degradation. The crystal structure, nanosize and magnetic properties of the synthesized catalyst were confirmed by FESEM, XRD, EDS, mapping, line scan, FTIR, BET and VSM analyses. The results showed the high efficiency of nanophotocatalyst in antibiotic degradation (96.88%) and mineralization (83.23%) under optimal conditions: catalyst dose 0.24 g/L, initial concentration 5 mg/L, pH 3 and 60 min. In addition, the removal performance of AgCoFe$_2$O$_4$@Ch/AC still reached 80.16% after four cycles, which indicates the high reusability of the nanocatalyst and its retention of metal ions. CFTR degradation followed a *pseudo*-first-order kinetics and Langmuir–Hinshelwood model with $R^2 \sim 0.92$. Irrigation of

lettuce, watercress, radish and tomato seeds with the effluent from the reactor showed the growth of the plants and the safety of the effluent for the environment. Due to its magnetic property, chemical stability, reusability and high efficiency, AgCoFe$_2$O$_4$@Ch/AC can be a suitable option in the destruction of antibiotics from industrial and hospital wastewaters. For future research, it can be suggested that different kinds of carbon structures such as graphene oxide, nanotube carbons, graphite, charcoal or various polysaccharide structures such as methylcellulose, carboxymethyl cellulose, starch or glucose can be used to modify various spinel metal ferrites to design functional magnetic nanohybrid catalysts. Modified spinel metal ferrites can be used in environmental remediation or catalysis for the removal of various organic and inorganic pollutants from contaminated water and wastewater. Also, the limitation statements include the following things that need more research in this field.

- Could the operating parameters of the photocatalytic process handle a larger volume of wastewater?
- Would the operating parameters be feasible for real applications?
- Could the catalyst effectively remove the pollutants if the concentration range differs?
- Is doing this process economically justified?

Author contributions MHAF involved in investigation, methodology and writing the original draft. AN involved in advising, conceptualization, methodology, writing—reviewing and editing, visualization and validation. HD involved in supervision, writing—reviewing and editing, visualization and validation.

Declarations

Conflict of interest The authors confirm that there is no conflict of interest to declare.

References

Alcaraz de la Osa R, Iparragirre I, Ortiz D, Saiz J (2020) The extended Kubelka-Munk theory and its application to spectroscopy. ChemTexts. 6:1–14

Amirmahani N, Mahdizadeh H, Seyedi N, Nasiri A, Yazdanpanah G (2023) Synthesis and performance evaluation of chitosan/zinc oxide nanocomposite as a highly efficient adsorbent in the removal of reactive red 198 from water. J Chin Chem Soc 70(4):869–878

Ariga K, Vinu A, Yamauchi Y, Ji Q, Hill JP (2012) Nanoarchitectonics for mesoporous materials. Bull Chem Soc Jpn 85(1):1–32

Chang Pitter JY, Zhong L, Hamdy RF, Preciado D, Behzadpour H, Hamburger EK (2022) Ceftriaxone use for acute otitis media: associated factors in a large U.S. primary care population. Int J Pediatr Otorhinolaryngol 160:111211

Chen X, Zhao Q, Li X, Wang D (2016) Enhanced photocatalytic activity of degrading short chain chlorinated paraffins over reduced graphene oxide/CoFe2O4/Ag nanocomposite. J Colloid Interface Sci 479:89–97

Daraei H, Toolabian K, Thompson I, Qiu G (2021) Biotoxicity evaluation of zinc oxide nanoparticles on bacterial performance of activated sludge at COD, nitrogen, and phosphorus reduction. Front Environ Sci Eng 16(2):19

Daraei H, Mittal A, Toolabian K, Mittal J, Mariyam A (2023) Study on the biodegradability improvement of 2,4 dinitrophenol in wastewater using advanced oxidation/reduction process with UV/SO(3)/ZnO. Environ Sci Pollut Res Int 30(9):22273–22283

Fard SG, Haghighi M, Shabani M (2019) Facile one-pot ultrasound-assisted solvothermal fabrication of ball-flowerlike nanostructured $(BiOBr)_x (Bi_7O_9I_3)_{1-x}$ solid-solution for high active photodegradation of antibiotic levofloxacin under sun-light. Appl Catal B 248:320–331

Firoozi M, Hashemi M, Narooie MR, Daraei H (2023) Evaluation of phenol degradation rate using advanced oxidation/reduction process (AO/RP) in the presence of sulfite and zinc oxide under UV. Optik 279:170787

Golestani N, Nasiri A, Hashemi M (2022) $CoFe_2O_4$@MC/AC as an efficient and recyclable magnetic nanohybrid adsorbent for the metronidazole removal from simulated wastewater: bioassays and whole effluent toxicity. Desalin Water Treat 280:312–329

Joshi NC, Gururani P, Gairola SP (2022) Metal oxide nanoparticles and their nanocomposite-based materials as photocatalysts in the degradation of dyes. Biointerface Res Appl Chem 12:6557–6579

Kamranifar M, Allahresani A, Naghizadeh A (2019) Synthesis and characterizations of a novel $CoFe_2O_4$@CuS magnetic nanocomposite and investigation of its efficiency for photocatalytic degradation of penicillin G antibiotic in simulated wastewater. J Hazard Mater 366:545–555

Karci A (2014) Degradation of chlorophenols and alkylphenol ethoxylates, two representative textile chemicals, in water by advanced oxidation processes: the state of the art on transformation products and toxicity. Chemosphere 99:1–18

Karungamye P, Rugaika A, Mtei K, Machunda R (2022) A review of methods for removal of ceftriaxone from wastewater. J Xenobiotics 12(3):223–235

Kestioğlu K, Yonar T, Azbar N (2005) Feasibility of physico-chemical treatment and advanced oxidation processes (AOPs) as a means of pretreatment of olive mill effluent (OME). Process Biochem 40(7):2409–2416

Khorsandi H, Teymori M, Aghapour A, Jafari S, Taghipour S, Bargeshadi R (2019) Photodegradation of ceftriaxone in aqueous solution by using UVC and UVC/H_2O_2 oxidation processes. Appl Water Sci 9:1–8

Khorsandi H, Teymori M, Aghapour AA, Jafari SJ, Taghipour S, Bargeshadi R (2019) Photodegradation of ceftriaxone in aqueous solution by using UVC and UVC/H_2O_2 oxidation processes. Appl Water Sci 9:1–8

Kichukova D, Spassova I, Kostadinova A, Staneva A, Kovacheva D (2022) Facile synthesized Cu–RGO and Ag–RGO nanocomposites with potential biomedical applications. Nanomaterials 12(12):2096

Kim JR, Kan E (2016) Heterogeneous photocatalytic degradation of sulfamethoxazole in water using a biochar-supported TiO_2 photocatalyst. J Environ Manage 180:94–101

Kumar A, Guo C, Sharma G, Pathania D, Naushad M, Kalia S et al (2016) Magnetically recoverable ZrO_2/Fe_3O_4/chitosan nanomaterials for enhanced sunlight driven photoreduction of carcinogenic Cr(vi) and dechlorination & mineralization of 4-chlorophenol from simulated waste water. RSC Adv 6(16):13251–13263

Kushlyk M, Tsiumra V, Zhydachevskyy Y, Haiduchok V, Syvorotka II, Sugak D et al (2019) Enhancement of the YAG:Ce, Yb down-conversion emission by plasmon resonance in Ag nanoparticles. J Alloy Compd 804:202–212

Li G, Wang Y, Mao L (2014) Recent progress in highly efficient Ag-based visible-light photocatalysts. RSC Adv 4(96):53649–53661

Long S, Martin T (1989) Determination of trace elements in waters and wastes by inductively coupled plasma-mass spectrometry: method 200. 8. version 4. 0. Environmental protection agency, Cincinnati, OH (USA)

López-Peñalver JJ, Sánchez-Polo M, Gómez-Pacheco CV, Rivera-Utrilla J (2010) Photodegradation of tetracyclines in aqueous solution by using UV and UV/H_2O_2 oxidation processes. J Chem Technol Biotechnol 85(10):1325–1333

Lu J, Cui Z, Deng X, Liang Z, Chai S, Fan J et al (2020) Rapid degradation of dimethoate and simultaneous removal of total phosphorus by acid-activated Fe (VI) under simulated sunlight. Chemosphere 258:127265

Majlesi M, Daraei H (2016) Preparation and adsorption properties of chitosan-bound Fe_3O_4 magnetic nanoparticles for phenol removal from aqueous solution. World Rev Sci Technol Sustain Dev 12(4):371–380

Malakootian M, Nasiri A, Asadipour A, Kargar E (2019) Facile and green synthesis of ZnFe2O4@ CMC as a new magnetic nano-photocatalyst for ciprofloxacin degradation from aqueous media. Process Saf Environ Prot 129:138–151

Malakootian M, Nasiri A, Heidari MR (2020) Removal of phenol from steel plant wastewater in three dimensional electrochemical (TDE) process using $CoFe_2O_4$@AC/H_2O_2. Z Phys Chem 234(10):1661–1679

Moussavi G, Pourakbar M, Shekoohiyan S, Satari M (2018) The photochemical decomposition and detoxification of bisphenol a in the VUV/H_2O_2 process: degradation, mineralization, and cytotoxicity assessment. Chem Eng J 331:755–764

Nasiri A, Tamaddon F, Mosslemin MH, Amiri Gharaghani M, Asadipour A (2019) Magnetic nano-biocomposite $CuFe_2O_4$@ methylcellulose (MC) prepared as a new nano-photocatalyst for degradation of ciprofloxacin from aqueous solution. Environ Health Eng Manag J 6(1):41–51

Nasiri A, Rajabi S, Hashemi M, Nasab H (2022) $CuCoFe_2O_4$@MC/AC as a new hybrid magnetic nanocomposite for metronidazole removal from wastewater: bioassay and toxicity of effluent. Sep and Purif Technol 296:121366

Nasiri A, Heidari MR, Javid N, Yazdanpanah G (2022a) New efficient and recyclable magnetic nanohybrid adsorbent for the metronidazole removal from simulated wastewater. J Mater Sci Mater Electron 33(33):25103–25126

Nasiri A, Malakootian M, Javid N (2022b) Modelling and optimization of lead adsorption by $CoFe_2O_4$@CMC@HZSM-5 from aqueous solution using response surface methodology. Desalin Water Treat 248:134–148

Nasiri A, Rajabi S, Hashemi M (2022c) CoFe2O4@ methylcellulose/AC as a new, green, and eco-friendly nano-magnetic adsorbent for removal of Reactive Red 198 from aqueous solution. Arab J Chem 15(5):103745

Nishioka H, Cho Y, Irie K, Kanamori M (2022) Ceftriaxone-associated encephalopathy in a patient with high levels of ceftriaxone in blood and cerebrospinal fluid. Int J Infect Dis 116:223–225

Priac A, Badot P-M, Crini G (2017) Treated wastewater phytotoxicity assessment using Lactuca sativa: focus on germination and root elongation test parameters. CR Biol 340(3):188–194

Rajabi S, Nasiri A, Hashemi M (2022) Enhanced activation of persulfate by $CuCoFe_2O_4$@ MC/AC as a novel nanomagnetic heterogeneous catalyst with ultrasonic for metronidazole degradation. Chemosphere 286:131872

Ramasamy B, Jeyadharmarajan J, Chinnaiyan P (2021) Novel organic assisted Ag-ZnO photocatalyst for atenolol and acetaminophen photocatalytic degradation under visible radiation: performance and reaction mechanism. Environ Sci Pollut Res 28:39637–39647

Sayadi MH, Ahmadpour N, Homaeigohar S (2021) Photocatalytic and antibacterial properties of Ag-$CuFe_2O_4$@ WO_3 magnetic nanocomposite. Nanomaterials 11(2):298

Sharma S, Umar A, Mehta SK, Ibhadon AO, Kansal SK (2018) Solar light driven photocatalytic degradation of levofloxacin using TiO 2/carbon-dot nanocomposites. New J Chem 42(9):7445–7456

Shokri M, Isapour G, Shamsvand S, Kavousi B (2016) Photocatalytic degradation of ceftriaxone in aqueous solutions by immobilized TiO_2 and ZnO nanoparticles: investigating operational parameters. J Mater Environ Sci 7(8):2843–2851

Takdastan A, Sadeghi H, Dobaradaran S, Ma L, Sorooshian A, Ravanbakhsh M et al (2020) Synthesis and characterization of γ-Fe_2O_3 encapsulated NaY zeolites as solid adsorbent for degradation of ceftriaxone through heterogeneous catalytic advanced oxidation processes. J Iran Chem Soc 17:725–734

Tamaddon F, Mosslemin MH, Asadipour A, Gharaghani MA, Nasiri A (2020a) Microwave-assisted preparation of $ZnFe_2O_4$@ methyl cellulose as a new nano-biomagnetic photocatalyst for photodegradation of metronidazole. Int J Biol Macromol 154:1036–1049

Tamaddon F, Nasiri A, Yazdanpanah G (2020b) Photocatalytic degradation of ciprofloxacin using $CuFe_2O_4$@ methyl cellulose based magnetic nanobiocomposite. MethodsX 7:100764

Yang J, Fang L, Li Z, Meng G, Jia Y, Jiang Y et al (2023) Insights into the formation of environmentally persistent free radicals during photocatalytic degradation processes of ceftriaxone sodium by ZnO/ZnIn2S4. Chemosphere 314:137618

Yazdanbakhsh A, Paseban A, Ghorbanpoor R (2016a) Inhibitory effects of the amoxicillin on treatment efficiency of synthetic wastewater in a sequencing batch reactor. J Univ Med Sci 7(3):669–682

Yazdanbakhsh AR, Daraei H, Rafiee M, Kamali H (2016b) Performance of iron nano particles and bimetallic Ni/Fe nanoparticles in removal of amoxicillin trihydrate from synthetic wastewater. Water Sci Technol J Int Assoc Water Pollut Res 73(12):2998–3007

Yazdanpanah G, Heidari MR, Amirmahani N, Nasiri A (2023) Heterogeneous Sono-Fenton like catalytic degradation of metronidazole by Fe_3O_4@HZSM-5 magnetite nanocomposite. Heliyon 9(6)

Ziashahabi A, Prato M, Dang Z, Poursalehi R, Naseri N (2019) The effect of silver oxidation on the photocatalytic activity of Ag/ZnO hybrid plasmonic/metal-oxide nanostructures under visible light and in the dark. Sci Rep 9(1):11839

Publisher's Note Springer Nature remains neutral with regard to jurisdictional claims in published maps and institutional affiliations.